Deducing the depth of origin of granulite xenoliths from zircon-rutile thermometry: a case study from Tanzania

Dusty Aeiker
Geology 394
Advisors: Dr. Roberta Rudnick,
Dr. Bill McDonough and
Dr. Phil Piccoli

Abstract

The zircon-rutile geothermometer of Watson et al. (2006) has been applied to granulite-facies xenoliths and high-grade surface metamorphic rocks from the Mozambique Fold Belt (MFB), Tanzania, in order to determine whether the xenoliths derived from the present-day lower crust or from near-surface granulite terranes. Diffusion of Ti in zircon is expected to be exceedingly slow and to reflect the temperatures at which the zircons grew. In contrast, Zr diffuses relatively rapidly in rutile, and, as cooling rates decrease, the blocking temperature of rutile systematically decreases. Thus, in granulites that experienced very slow cooling (such as those in the present-day lower crust), Zr-in-rutile temperatures should be significantly lower than the temperatures recorded by coexisting zircons. In contrast, granulite-facies rocks found at or near the surface experienced uplift during the final phase of the orogeny, and may have cooled at a markedly faster rate (5 to 10 °C/m.y.). In this case, zircon and rutile are expected to return similar temperatures (i.e., within 30-50 °C, assuming a peak T of 800 °C). Zr in rutile was measured using EPMA and Ti in zircon using LA-ICP-MS from three granulite-facies xenoliths carried in rift-related basalts erupted through the MFB (two from the Kisite locality) and on the margin of the Tanzanian craton (one from the Labait locality). The two xenoliths from the MFB show contrasting results: a gt-bio orthogneiss yields zircon temperatures ranging from 780 to 1030 °C (mean = 850 ± 84 °C, 1σ), which are significantly higher than those recorded in coexisting rutile (590 to 750 °C, mean = 680 ± 42 °C). In contrast, a gt-opx mafic granulite from Kisite yields zircon and rutile temperatures that are indistinguishable from each other at 780 ± 30 °C; these temperatures are also notably cooler than those from the zircon in the gt-bio orthogneiss. It thus appears that the

orthogneiss derived from the present-day lower crust (and cooled very slowly from high T), while the gt-opx granulite may have derived from a near-surface metamorphic terrane that experienced overall lower metamorphic temperatures and more rapid cooling. Although no high-grade metamorphic rocks crop out in the vicinity of Kisite, they do occur ~45 km to the east. The sample from the craton margin (Labait locality) is a mafic, gt-opx granulite that yields zircon temperatures ranging from 900 to 1020 °C (mean = 960 ± 44 °C). These T's are significantly greater than those returned from coexisting rutile (620 to 785 °C, mean = 640 ± 45 °C), suggesting that this xenolith is also a sample of present-day lower crust that formed at very high temperatures and cooled slowly in the lower crust of the Tanzanian craton. A graphite schist surface sample from the MFB yields zircon temperatures from 690 to 940 °C (mean = 800 ± 76 °C), which overlap the temperatures recorded by the rutile (750 to 810 °C, mean = 791 ± 11 °C). The large range in zircon temperatures could reflect multiple populations of zircons (detrital and metamorphic), so it is difficult to deduce a cooling history and origin for this rock without more information on the origin of the zircon. A gt-rutile amphibolite surface sample from another locality within the MFB yields rutile temperatures that range from 650 to 750 °C (mean = 714 ± 23 °C). Zircon temperatures are quite variable, ranging from 710 to 1020 °C (mean = 824 ± 121°C), which may be due to different populations of zircons (e.g. igneous versus metamorphic zircons). Variations within the time-resolved Ti spectra for some zircons suggest the presence of different temperature domains within a single crystal. Further investigation into the reason for the variable Ti temperatures for zircon from the two surface samples is required before any conclusions can be made.

Table of Contents

1. Introduction

The Mozambique Fold Belt (MFB) of East Africa was generated by the Pan-African Orogeny: the late Neoproterozoic collision of East and West Gondwana. Due to a lack of reliable geochronological and thermobarometry data, there is still much uncertainty surrounding the evolution of the MFB and the chronology of the geologic events of the Pan-African.

To the west of the MFB lies the Archean Tanzanian craton. This stable craton has resisted several collisions that formed the complex system of mobile belts surrounding it. It is also bounded by the eastern and western branches of the East African Rift system. Weeraratne et al. (2003) suggest that the Tanzania craton's resistance to the rifting stopped the eastern branch from propagating southward when it came into contact with the craton, causing the rifting to continue on the western border of the craton.

Due to the rifting, my study area, along the eastern Tanzanian craton border, has experienced an increase in volcanism. The rifting created breaks in the crust from which magma escaped and carried pieces of the crust underlying the MFB to the surface. Pieces of the crust (or mantle) that become entrained in magma and are rapidly brought to the surface are termed xenoliths. The xenoliths collected from my study area can be used to understand the tectonic and thermal history of the MFB by providing information about the conditions of the crust from which they were derived. In order to understand the tectonics of the MFB in Tanzania, it is necessary to compare the thermal history of the present-day lower crust with that of the upper crust. However, further investigations of the MFB, such as thermochronology investigations using U-Pb dating of rutile and zircon, cannot proceed until the source of the granulite xenolith samples is better constrained. This project uses the zircon-rutile thermometers developed by Watson et al. (2006) to

distinguish between xenoliths that are derived from the present-day lower crust versus those derived from near-surface granulite terranes by comparing the temperatures recorded by zircon to those recorded by coexisting rutile.

The temperatures calculated from the Zr-in rutile thermometer are susceptible to diffusive re-equilibration, which enables us to determine the temperature-time path of each sample. The thermodynamic basis is the reaction $TiO_{2\ (rutile)} = TiO_{2\ (zircon)}$ for the Ti-in-zircon thermometer and $ZrO_{2\ (zircon)} = ZrO_{2\ (rutile)}$ for the Zr-in-rutile thermometer. Diffusion of Ti in zircon and Zr in rutile is a function of temperature. According to Watson et al. (2006), Ti should diffuse exceedingly slowly in zircon. Therefore, when the zircon cools, it retains most of the Ti that was incorporated into its crystal structure during crystallization. Although the diffusion rate of Ti in zircon has not been measured, Watson assumed it is slow based on the very slow diffusion of other 4^+ trace elements in zircon such as Hf.

Conversely, Zr in rutile diffuses relatively rapidly and could potentially reset the recorded metamorphic temperature during slow cooling. Rutile crystals will lose Zr until the blocking temperature of the rutile grain is reached (Fig. 1). Blocking temperature is a function of both grain size and cooling rate. As the cooling rates decrease, the blocking temperatures systematically decrease, thus, the period of time during which the Zr is able to diffuse out of the rutile crystal increases. The same is true for smaller crystals versus larger crystals. Smaller crystals have lower blocking temperatures than larger crystals and will record lower temperatures.

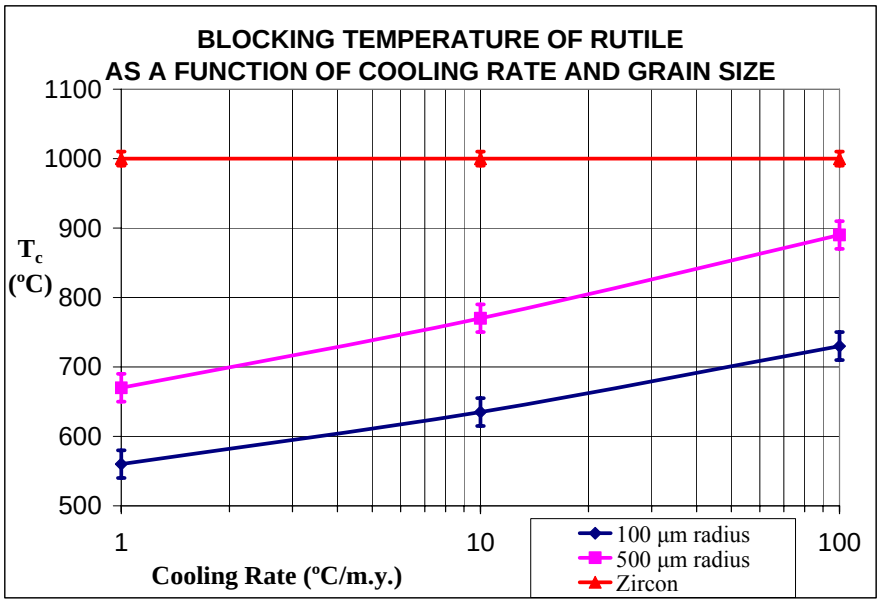

Fig. 1. Blocking temperature (T_c) shown as a function of cooling rate and grain size. The radii of the rutile grains analyzed in my study ranged in size from 50 -500 µm.

Assuming that granulite-facies rocks that crop out at or near the surface in the MFB were uplifted during the terminal phase of the orogeny, they would have cooled more rapidly than granulites that cooled isobarically in the lower crust. A rutile crystal that experienced a slower cooling rate, such as during isobaric cooling in the lower crust, will have a lower blocking temperature and record a lower temperature than one that experienced rapid uplift, allowing it to cool more rapidly. This is also assuming that all orogenic heat has dissipated since the orogeny and that the present geotherm of the MFB crust is relatively cool. The cool geotherm ensures that the rutile crystals would actually reach their blocking temperature if cooled within the lower crust. Therefore, the difference in temperatures recorded by coexisting zircon and rutile in the granulites that were exhumed should be smaller than the difference in temperatures recorded by zircon and rutile in granulites that have experienced isobaric cooling within the lower crust. Peak metamorphic temperatures recorded by the zircons between the upper and lower

crust may also vary. This would be the result of the more intense heating that might have occurred in the lower crust due to basaltic underplating.

2. Background

2.1. Granulite-facies

The predominant rock types of the MFB in Tanzania are granulites and amphibolites. Peak metamorphic conditions of the MFB resulted in granulite-facies rocks (high grade metamorphic rocks) that retrograded into amphibolite and greenschist-facies rocks in some areas (Fig. 2). This particular sequence of metamorphic facies, greenschist to amphibolite to granulite-facies, is characteristic of orogenic belts and is part of what is often referred to as the medium P-T series (Fig. 3). Although the origin of granulite-facies rocks is still debated, there is a general consensus regarding the temperatures associated with the formation and the amount of water present in granulite-facies rocks. The granulite-facies is indicative of temperatures greater than 700 °C but record pressures that are typical of 500 °C when following an average geotherm. This suggests that granulite-facies rocks are produced during continent-continent collisions in which the crust is thickened (Winter, 2001).

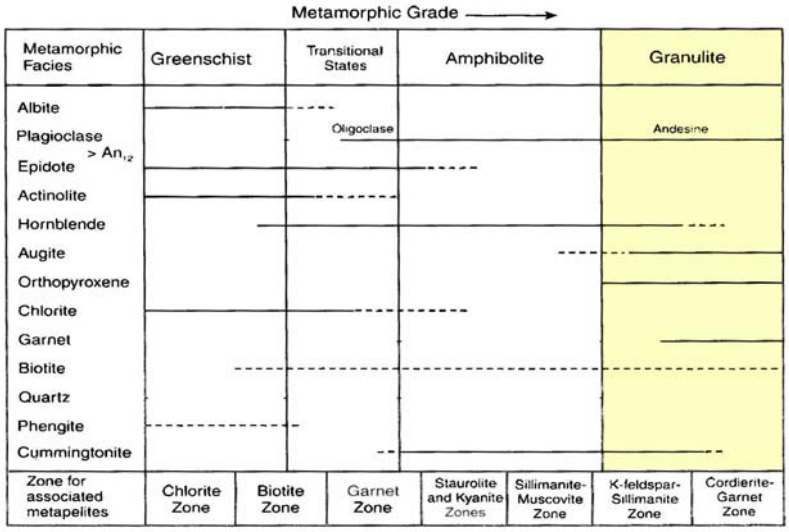

Fig. 2. A chart illustrating the changes in mineral assemblages of metabasic rocks during metamorphism. The sequence depicted, greenschist amphibolite, granulite, is known as the medium P-T series, characteristic of most orogenic belts. Figure taken from An Introduction to Igneous and Metamorphic Petrology (Winter, 2001).

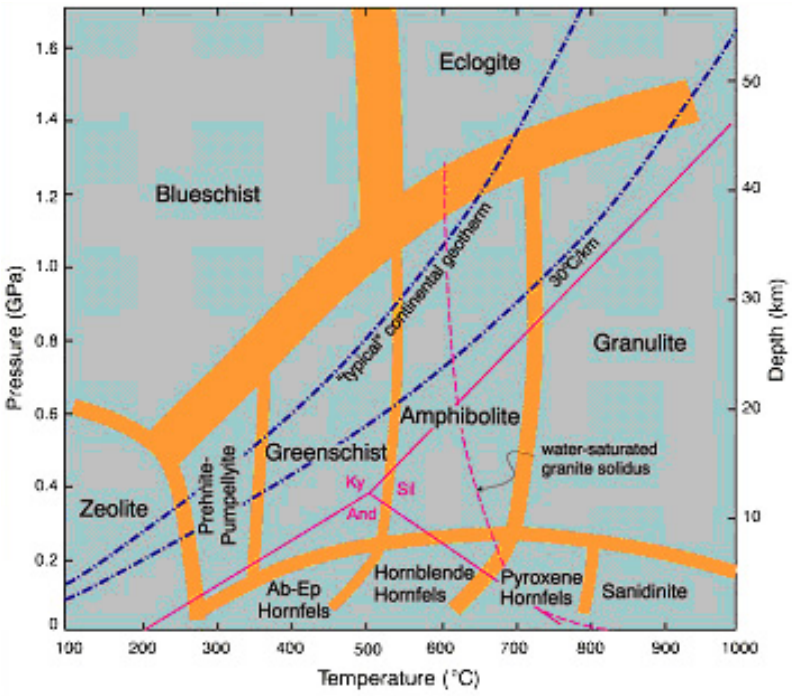

Fig. 3. Temperature-pressure diagram showing the various metamorphic facies coined by Eskola and several others that are commonly used. Also plotted:

- the "typical" continental geotherm
- a 30 ºC/km geotherm (an example of an elevated orogenic geotherm)
- the Al_2SiO_5 polymorphs' stability ranges
- melting curve for H_2O saturated granite

Figure taken from An Introduction to Igneous and Metamorphic Petrology (Winter, 2001).

Granulite-facies rocks are also characterized by anhydrous mineral assemblages. The absence of water may prevent the rocks from melting. Alternatively, granulites may be residues of melting in which the water left with the melt. The diagnostic mineral assemblage of granulite-facies mafic rocks is orthopyroxene + clinopyroxene + plagioclase ± garnet ± hornblende (Winter, 2001). This mineral assemblage is typical of what we see in the granulite-facies xenoliths collected from the vicinity of the MFB in Tanzania.

2.2 Pan-African Orogeny

The thickening of the crust during the Neoproterozoic Pan-African Orogeny likely formed the MFB granulites. Between ~700-500 Ma the continent of Africa formed through the collisions of many small continents. The orogenies that sutured these continents together are known as the Pan-African Orogeny, which ended approximately 500 Ma ago (Stanley, 1999).

3. Geologic Setting

The MFB (Fig. 4) is an orogenic belt that runs north-south through Eastern Africa, from Sudan and Ethiopia to the southern region of Mozambique. The MFB of Tanzania is characterized by a 1,000 km stretch of discontinuous high-grade granulite and gneiss facies. Peak metamorphism in the MFB of Tanzania resulted in granulite-facies conditions, but in some areas the granulite terranes have retrograded to amphibolite and greenschist-facies. Several granulite-facies surface outcrops occur within the mobile belt. Appel et al. (1998) and Sommer et al. (2003) assert that the surface granulites followed a clockwise P-T path, although there is still debate about this (Fig. 5). Schenk et al. (2005), for example, argue that the Congo craton's eastern boundary in Tanzania followed an anticlockwise P-T path, which suggests very strong heating prior to the collision of east and west Gondwana. The granulite-facies metamorphism in the northern MFB of Tanzania has been dated at 640 Ma using zircon dating techniques such as U-Pb SHRIMP (Sensitive High Resolution Ion MicroProbe) and Pb-Pb evaporation (Muhongo et al., 2001; Sommer et al., 2003). Sommer et al. (2003) calculated peak metamorphic temperatures of 800 ± 20 °C and pressures that range from 8-15 kbar.

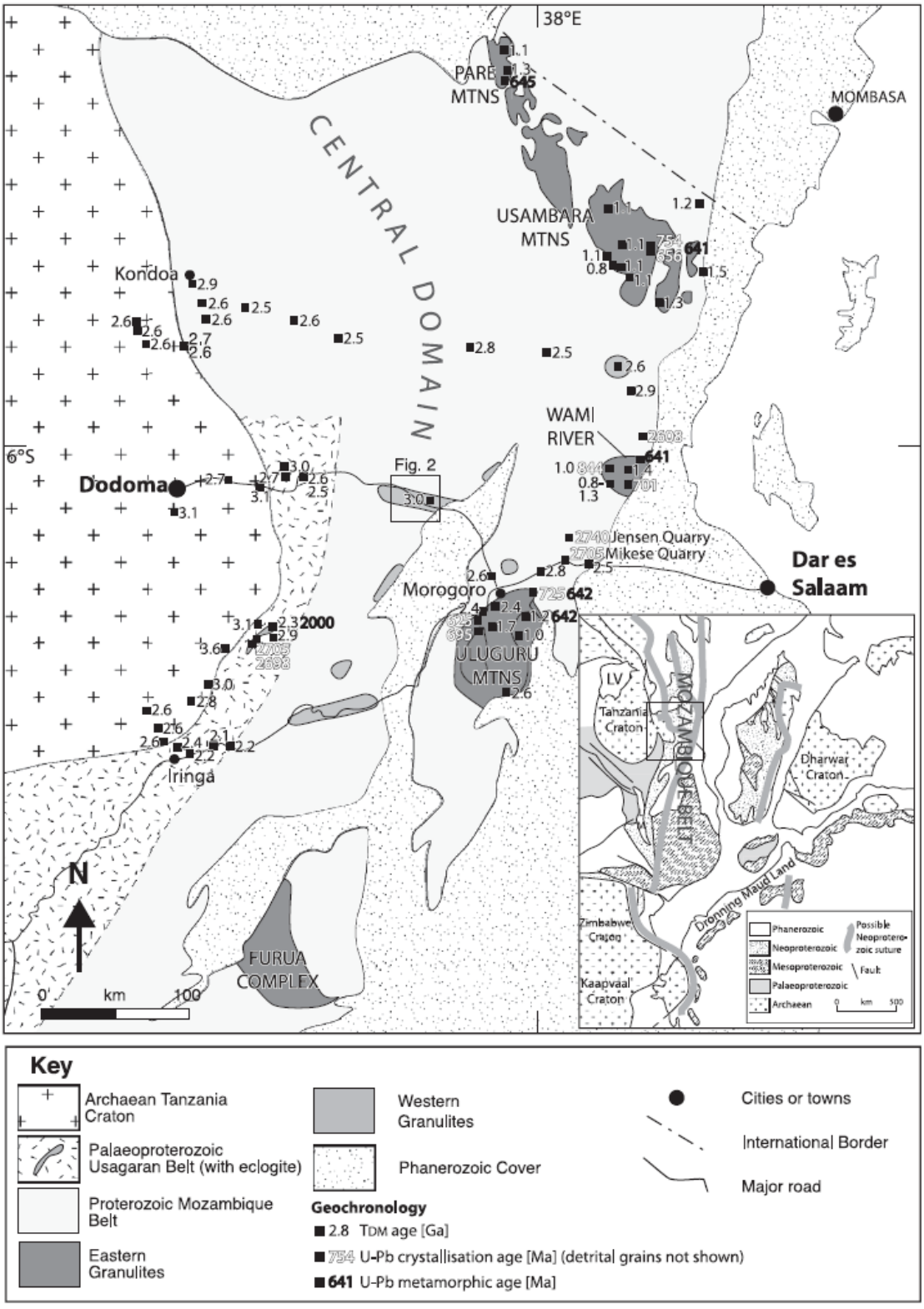

Fig. 4. Map of the MFB in Tanzania taken from (Johnson et al. 2003).

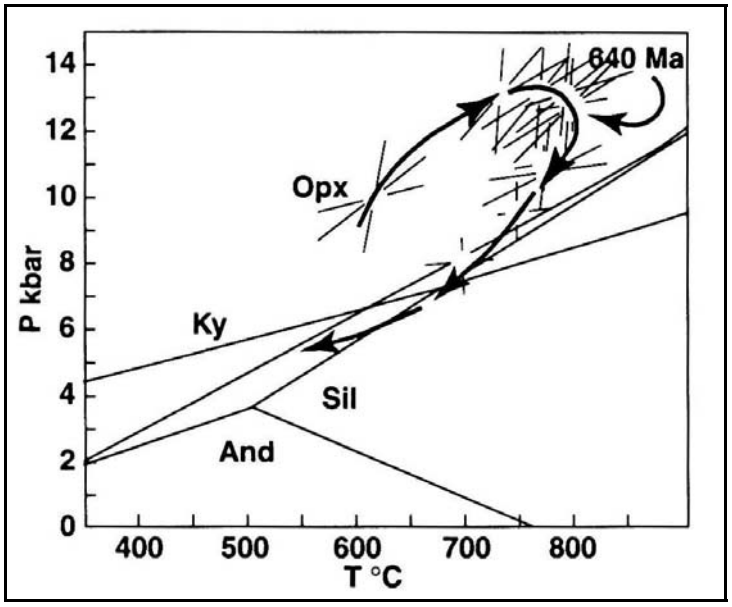

Fig. 5. Clockwise P-T path for granulite facies rocks from central MB of Tanzania. Granulite facies metamorphism occurred at temperatures of 800 ± 20 ºC, and was dated at *c.* 640 Ma. (Sommer et al. 2003).

The MFB runs along the western border of the Tanzanian Craton; a 350,000 km^2 stable craton composed of greenstone belts and granitoids that date back to approximately 2800 Ma. The Tanzanian Craton is situated between the eastern and western branches of the East African Rift (Weeraratne et al. 2003). Volcanism associated with the rifting carried both upper mantle and crustal xenoliths to the surface, but this study will focus on the crustal xenoliths. The xenoliths are primarily in the granulite-facies.

4. Samples

Thin sections were made from the xenolith and surface samples collected from the MFB of Tanzania in 2004 and 2006. Of the thin sections, three xenolith samples and two surface samples contained coexisting rutile and zircon. Polished thin sections were used for Electron Probe Microanalyzer (EPMA) and Laser Ablation-Inductively Coupled Plasma-Mass Spectrometer (LA-ICP-MS) analyses. Two polished thin sections, a xenolith sample and a surface sample, were also used for cathodoluminescence (CL) imaging. Figures 6-9 show the surface sample and xenolith localities. Labait is located

on the margin of the Tanzanian craton, and Kisite and the surface samples are located within the MFB.

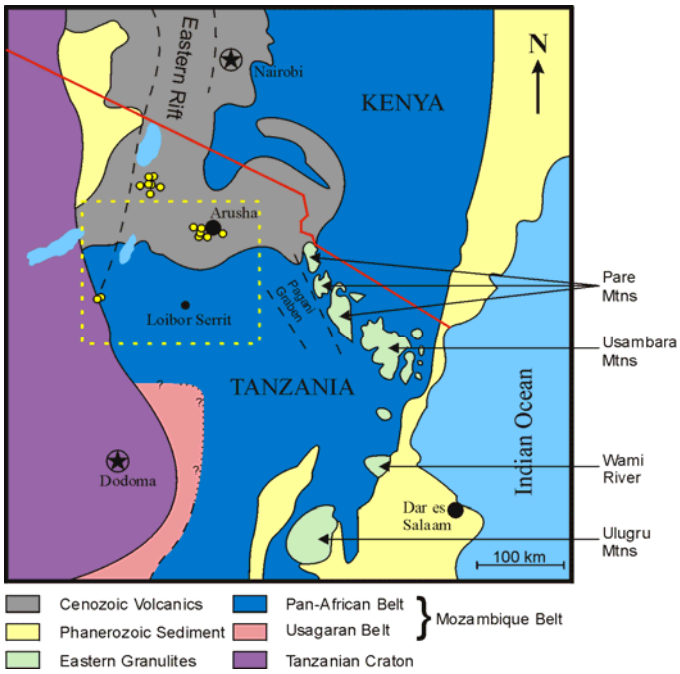

Fig. 6. Geologic map of northern Tanzania showing the location of Arusha and other sample sites. Surface samples were collected from sites that fall within the area enclosed by the dashed yellow line, including Loibor Serrit and Lolikisale. The yellow dots are xenolith localities, including Labait and Kisite.

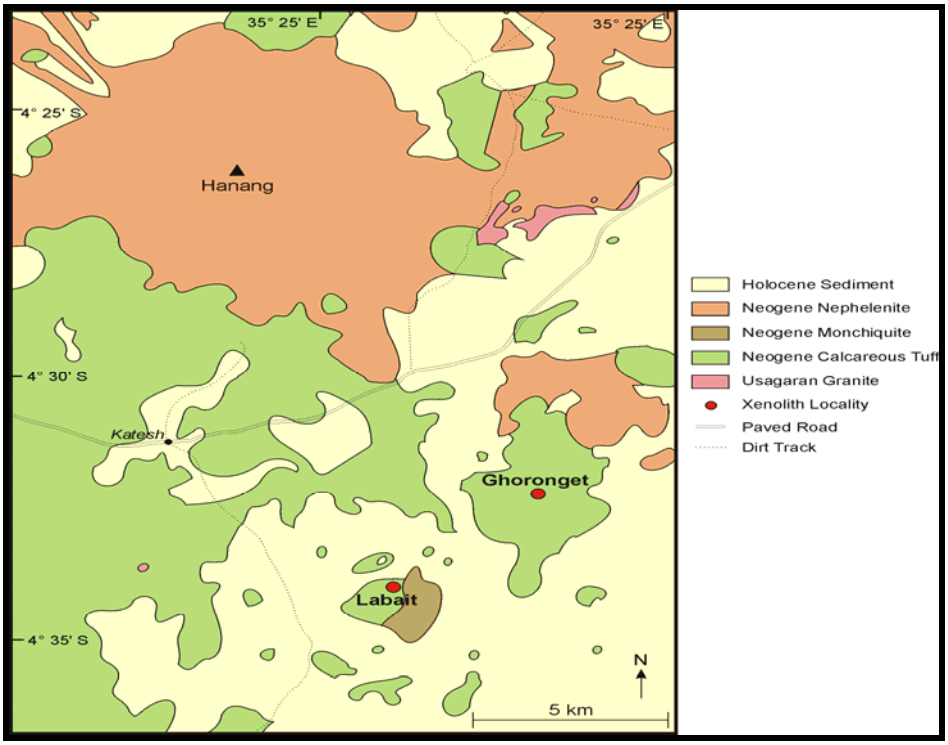

Fig. 7. Map of Labait volcano, located at S4^{o}22.9' E35^{o}26.2' created by Sean Timpa. There were many cumulate and residual peridotites, some garnet-bearing and abundant crustal xenoliths. Dr. Rudnick and her colleagues originally thought crustal xenoliths were rare, but discovered otherwise when they revisited this area in 2004. Most are two pyroxene granulites, some with garnets.

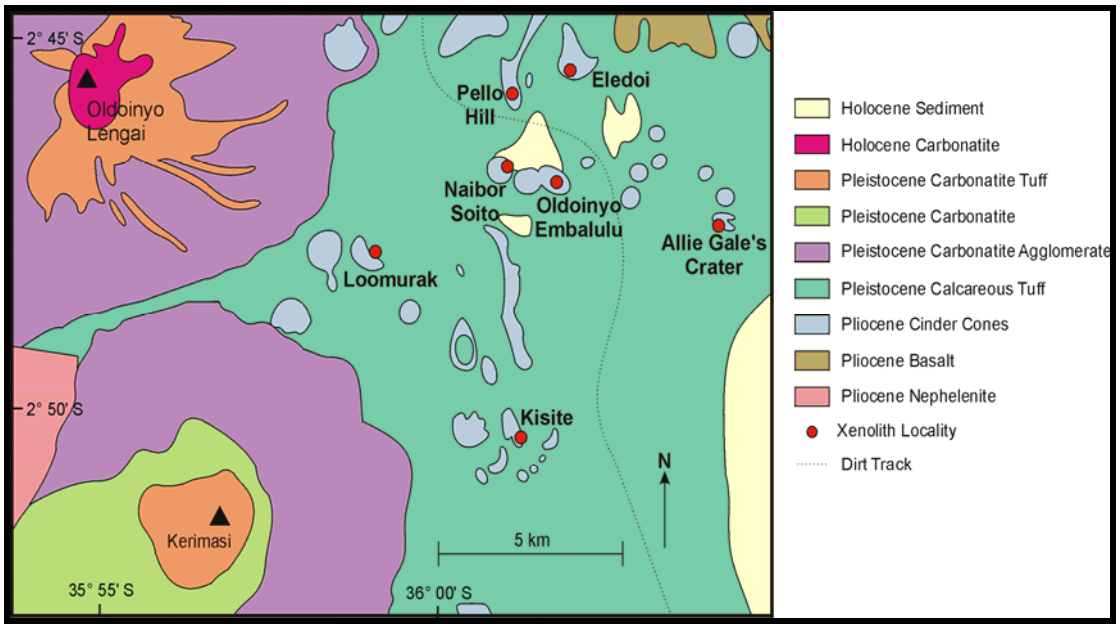

Fig. 8. Map of sites in the vicinity of Oldoinyo Lengai volcano created by Sean Timpa. Kisite is located in the south eastern quadrant of the map.

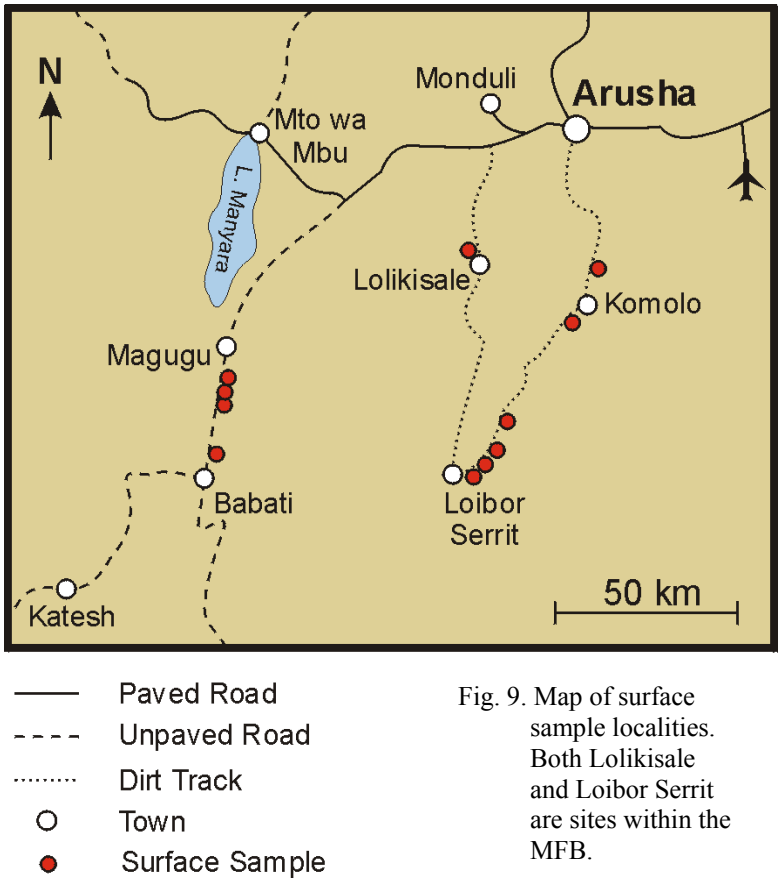

Fig. 9. Map of surface sample localities. Both Lolikisale and Loibor Serrit are sites within the MFB.

4.1. Xenolith samples

From my EPMA analyses, I have found that the rutile crystals in the granulite xenoliths are occasionally associated with ilmenite occurring either as rims and/or exsolution lamellae (Fig. 10). This was true for rutile in the mafic garnet-orthopyroxene granulites from Labait and Kisite (LB04-91 and KS04-01 respectively), the garnet-biotite orthogneiss from Kisite (KS04-03), and the garnet amphibolite from Lolikisale (LO06-01). Several rutile specimens in samples LB04-91, KS04-03, and LO06-01 exhibit exsolution of a Zr-rich phase, which may be zircon (but it was too small to analyze properly).

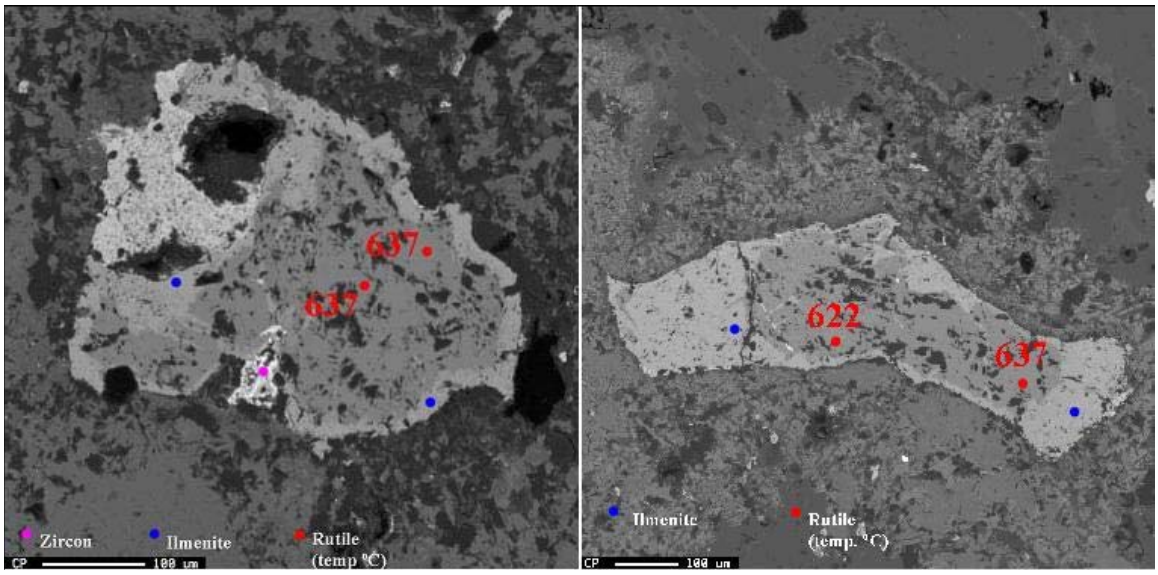

Fig. 10. Backscatter electron images of grain 3 (left) and 4 (right) from sample LB04-91. Note the lighter ilmenite rims, the darker gray rutile core, and the possible zircon exsolution. Numbers indicate calculated temperature for that spot analysis.

4.1.1. Mafic garnet-orthopyroxene granulite from Labait (LB04-91)

This granulite has a weakly gneissic texture and is moderately altered. Its mineral assemblage consists of plagioclase, quartz, garnet, orthopyroxene, potassium feldspar, rutile, opaque minerals, zircon, and apatite. Trace amounts of slightly altered rutile that range in size from 0.1 - 0.5 mm in diameter are present. Many of the rutile crystals occur

as inclusions in garnet (Fig. 11). There are a few zircons that are approximately 100 μm in diameter.

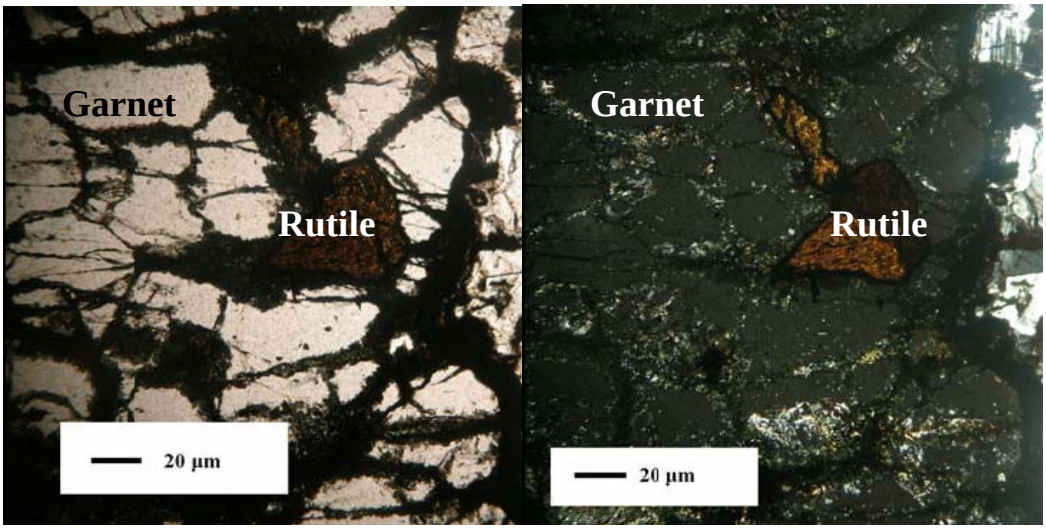

Fig. 11. Rutile grain from the mafic garnet-orthopyroxene granulite xenolith from Labait (sample LB04-91) in ppl and xpl under 4x magnification.

4.1.2. Garnet orthogneiss from Kisite (KS04-03)

This highly altered orthogneiss contains plagioclase, quartz, garnet, biotite, rutile (modal abundance = 1%), apatite, and zircon. The majority of the rutile crystals have a diameter between 0.5 mm – 100 μm. Trace amounts of zircon, approximately 100 μm in diameter, are also present.

4.1.3. Mafic garnet-orthopyroxene granulite from Kisite (KS04-01)

This granulite is slightly altered, and infiltration of the host magma has occurred along fractures. It contains quartz, plagioclase, garnet, biotite, orthopyroxene, opaque minerals, potassium feldspar, rutile (modal abundance = 1%), and zircon. The rutile grains are approximately 500 μm in diameter. There are a few zircons that are ~100 μm in diameter.

4.2. Surface samples

As with the xenolith samples, several of the rutile crystals analyzed on the EPMA display ilmenite exsolution in the form of lamellae and the exsolution of a Zr-rich phase in the form of little blobs.

4.2.1. Graphite Schist from Loibor Serrit (LR04-04)

This schist is a highly altered, strongly foliated, graphite schist. Its mineralogy consists of quartz, plagioclase, muscovite, graphite, and contains trace amounts of rutile, apatite, and zircon. The zircon and rutile crystals are roughly 50 and 100 μm in diameter, respectively.

4.2.2. Garnet amphibolite from Lolikisale (LO06-01)

This sample is a foliated amphibolite that contains amphibole, quartz, plagioclase, garnet and trace amounts of zircon and rutile. The zircon crystals are approximately 20 to 40 μm in diameter, and the rutile crystals range in size from 40 μm to 1 mm in diameter.

5. Analytical Techniques

5.1. Electron Probe Microanalyzer

JEOL JXA-8900R Electron Probe Microanalyzer (EPMA) at the University of Maryland, College Park, was used for the analyses of Zr in rutile, and Hf content of zircon, which will be used as an internal standard for LA-ICP-MS analyses. The operating conditions used for the all EPMA analyses (Nov. 4-5, 2005 and Mar. 24, 2006) were as follows:

- Accelerating voltage: 15 keV
- Cup current: 150 nA
- Beam size: 5 μm diameter

The samples analyzed consisted of polished thin sections, and were coated with ~300 angstroms of carbon using standard thermal evaporation techniques. The elements selected for rutile analyses on November 4 and 5, 2006 included the following: Fe, Mn, Nb, Ti, and Zr. The standards for the rutile analyses were a natural rutile crystal (Ti, Fe), ilmenite (Mn, Nb), kyanite (Al), and synthetic zircon (Zr). Fe, Ti, and Zr were used for rutile analyses on March 24, 2006. Fe and Zr were selected to identify ilmenite rims and lamellae and Zr exsolution. Zr, Hf, and Si were the elements selected for all zircon analyses. The Ti content of the zircons was not measured using the EPMA because concentrations are generally too low to detect. Standards for the zircon analyses consisted of synthetic zircon (Zr, Si) and hafnon (Hf). The advantage of using the EPMA for analyses is its spatial resolution. For example, Watson et al. (2006) found dramatically increased levels of Zr on the rims (a traverse of roughly 25 μm) of rutile from one of the peridotite xenoliths from Labait that reflect a heating event. Backscatter electron images of the rutile and zircon crystals from the granulites were taken to look for zoning.

5.2. Laser Ablation-Inductively Coupled Plasma-Mass Spectrometer (LA-ICP-MS)

Ti in zircon was measured on the Element 2, an inductively coupled mass spectrometer at the University of Maryland. The Element 2 has a single electron multiplier detector that can detect most elements, except noble gases from Li to U, and has a rapid scanning magnet, so it can produce time resolved analyses. Its low detection limit allows us to measure the abundance of certain elements to the ppq (parts per quadrillion) level, although Ti concentrations are not expected to be that low in my samples. Measured isotopes include ^{49}Ti, ^{91}Zr, ^{178}Hf, and ^{179}Hf. The NIST 610 glass, a well characterized glass reference material containing a wide range of elements (including Zr, Hf, and Ti) with concentrations of approximately 400 ppm, was used as an

external standard. Hf measurements from EPMA analyses were used as the internal standard. Measuring Ti concentrations using the LA-ICP-MS proved to be a challenge due to several factors including very low Ti concentrations (Fig. 12), Hf counts going off-scale, and isobaric interferences.

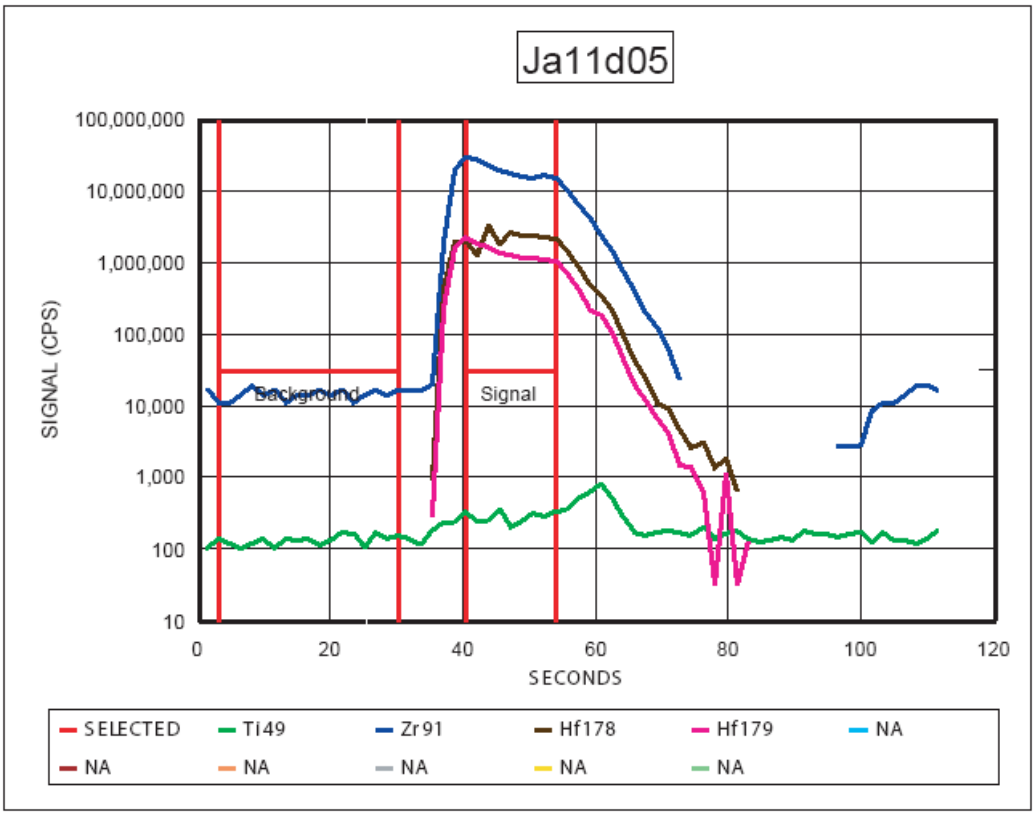

Fig. 12. Time-resolved spectrum of a zircon analysis. The zircon was from the mafic garnet-orthopyroxene granulite xenolith from Kisite (KS04-01). Note the high signal for ^{91}Zr, ^{178}Hf, ^{179}Hf, and the very low signal of ^{49}Ti barely above background corresponding to a concentration of 12 ppm.

5.2.1. Challenges Using the LA-ICP-MS

Measuring the low Ti concentrations was problematic due to isobaric interferences, particularly doubly charged Zr. Where an isotope appears in the mass spectrum depends on its charge and its mass. Most elements are ionized to singly charged species, but a small percentage become doubly charged (e.g. Zr^{2+} instead of Zr^{+}). Because the charge is doubled, the isotope experiences twice the attraction of the electrostatic field within the magnet as it would if it were singly charged. This means

that doubly charged ions appear at half the mass as the singly charged ions. So $^{92}Zr^{2+}$ would appear at half of 92 or mass 46, etc. (Table 1). ^{49}Ti and ^{50}Ti are the only two Ti isotopes without interference from doubly charged Zr, but even for these isotopes other isobars do exist. Isobars at ^{49}Ti include $^{98}Mo^{2+}$, and isobars at ^{50}Ti include ^{50}V, ^{50}Cr, $^{100}Mo^{2+}$, $^{100}Ru^{2+}$ (Table 2). ^{49}Ti was analyzed because this particular isotope has the least number of isobaric interferences. However, other caveats arise when measuring this isotope. Although ^{49}Ti has the least isobaric interferences, its abundance is relatively low in comparison to most other Ti isotopes (Table 1). This compounds the initial problem of Ti concentrations being very low in zircon. Thus, large spot sizes and relatively high laser frequencies are required to measure the Ti concentrations, which dramatically reduces the spatial resolution. The limitation of spatial resolution constrains our ability to measure Ti concentrations in different zones within the zircon and observe the variability of Ti throughout the crystal. Cathodoluminescence imaging did provide evidence of zoning in the zircons from the garnet-biotite orthogneiss xenolith from Kisite, sample KS04-03, and in the garnet amphibolite surface sample from Lolikisale, sample LO06-01 (cathodoluminescence imaging was not conducted on zircons from the mafic garnet-orthopyroxene granulites from Labait, sample LB04-91, and Kisite, sample KS04-01, and the graphite schist from Loibor Serrit, sample LR04-04). Variations in Ti within the time-resolved spectra were observed in zircons from the garnet-biotite orthogneiss xenolith from Kisite and the garnet amphibolite surface sample from Lolikisale. These variations were interpreted as Ti zoning (e.g. Fig. 13). Zircons from the other three samples displayed very little, if any, variation within the time-resolved Ti spectra.

Table 1. Doubly charged Zr interferences with Ti isotopes

Zr^{+} mass	Zr^{2+} mass	Ti^{+} mass	Ti Abund. (%)
90	45		
91	45.5		
92	46	46	8
94	47	47	7.3
96	48	48	73.8
--	--	**49**	**5.5**
--	--	50	5.4

Masses of singly and doubly charged Zr isotopes (as read by the LA-ICP-MS), the corresponding Ti isotope that they interfere with in ICP-MS analyses, and the relative abundances of the different Ti isotopes. ^{49}Ti was selected for zircon analyses, which has a relatively low abundance compared to other Ti isotopes.

Table 2. ^{49}Ti and ^{50}Ti isobars

Ti^{+} mass	Isobars	Isobar Abund. (%)
49	**$^{98}Mo^{2+}$**	**24**
50	^{50}V	0.2
	^{50}Cr	4.3
	$^{100}Mo^{2+}$	9.7
	$^{100}Ru^{2+}$	17

^{49}Ti and ^{50}T i do not have interference from doubly charged Zr, but they do have other isobars. $^{98}Mo^{2+}$ interferes with ^{49}Ti analyses.

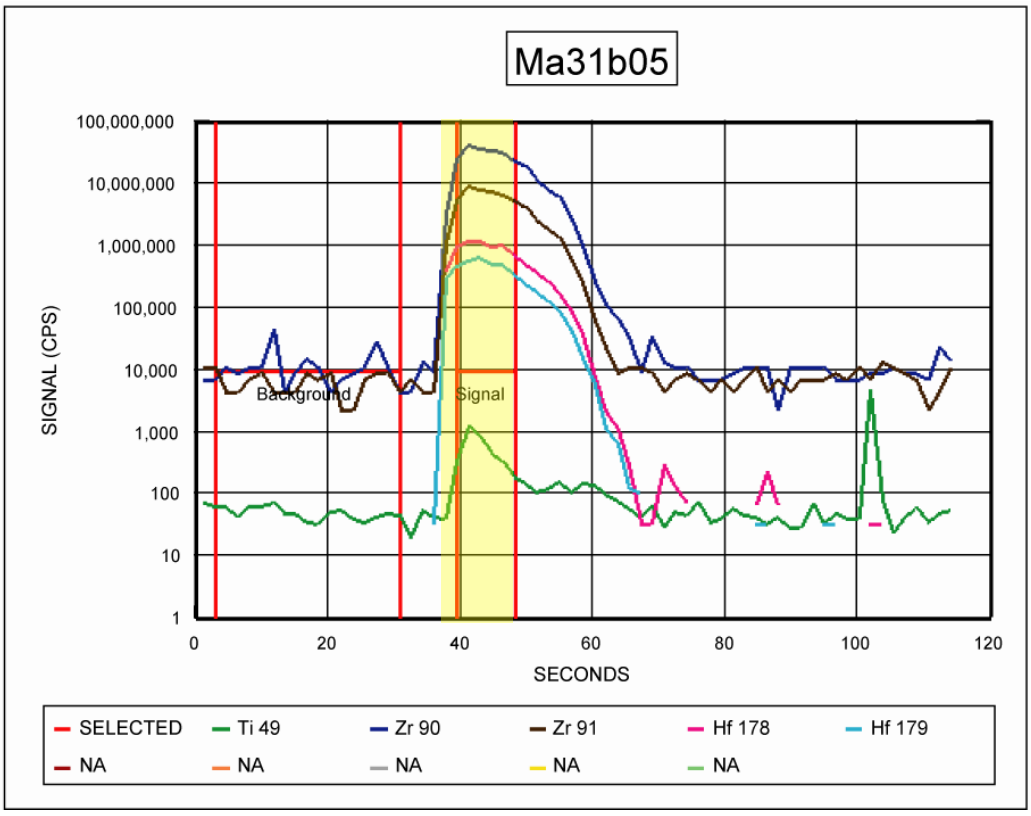

Fig. 13. Time-resolved spectrum of a zircon analysis. The zircon is from the garnet amphibolite surface sample from Lolikisale (LO06-01). Note the ^{49}Ti peak within the highlighted area that corresponded to a concentration of 118 ppm. This was interpreted as an igneous core.

Additional problems arose during the ablation of zircons from the mafic garnet-orthopyroxene granulite xenolith from Kisite. As a consequence of using high laser frequencies, counts for both ^{179}Hf and ^{178}Hf, the internal standard, were very high and often went off-scale. However, using lower laser frequencies resulted in Ti counts that barely rose above the background. These extremely low concentrations of Ti could not be measured accurately, so temperatures could not be calculated. Situations in which both Hf isotopes went off-scale, ^{91}Zr (measured in the analog detection mode because of its relatively high abundance) was used as the internal standard.

5.3. Cathodoluminescence (CL) Petrography Techniques

When bombarded by electrons, certain materials emit light called cathodoluminescence (CL). The color and intensity of cathodoluminescent signals can be used to determine trace element chemistry of minerals and is useful for distinguishing zoning in crystals. I used CL imaging to identify Ti zoning in zircons. Representative zircon crystals from the garnet-biotite orthogneiss xenolith from Kisite and the garnet amphibolite surface sample from Lolikisale were selected for imaging. Different zones could potentially contain different Ti concentrations, reflecting different growth conditions of the zircon. Ideally, we wanted to ablate a single zone and use a Hf concentration measured within that same zone as the internal standard in order to accurately determine the Ti content. The selected specimens were photographed with an Olympus Opelco MagnaFire Model S99806 camera system mounted on a microscope attached to a Premier American Technologies luminoscope model ELM-3R. The device is located in the Department of Mineral Sciences, National Museum of Natural History, Smithsonian Institution and was used with the help of Dr. Sorena Sorensen. These images were used to navigate around the zircons of the garnet-biotite orthogneiss xenolith from

Kisite and determine where it should be ablated (that is if the crystal was large enough to accommodate more than one spot analysis). CL images of the zircons from the garnet amphibolite surface sample from Lolikisale were taken after the crystals were ablated and were used to confirm our speculations of Ti zoning in the zircons.

5.4. Calculations

The following equations from Watson et al. (2006) were used to calculate the temperatures of the zircons and rutiles:

$T\ (°C)_{zircon} = (5080 \pm 30)/\ [(6.01 \pm 0.03) - \log (Ti)] - 273$

$T\ (°C)_{rutile} = (4470 \pm 120)/\ [(7.36 \pm 0.10) - \log (Zr)] - 273$

(Ti and Zr are expressed in ppm)

From the calculated temperatures cooling histories were deduced based on the difference in temperatures recorded by the zircons and rutiles in each sample.

6. Results and Discussion

6.1. Xenolith Sample Zircon and Rutile Temperatures and Interpretations

Maximum, minimum, average and median temperatures calculated for zircon and rutile from each sample are listed in Table 3.

Table 3. Temperatures returned by zircon and rutile

RUTILE

Sample No.	T_{max} (°C)	T_{min} (°C)	T_{ave} (°C)	Std. dev.(°C)
LB04-91	785	553	662	71
KS04-01	794	751	769	18
KS04-03	749	590	676	52
LR04-04	810	754	788	14
LO06-01	765	651	710	27

ZIRCON

Sample No.	T_{max}(°C)	T_{min}(°C)	T_{ave}(°C)	Std. dev.(°C)
LB04-91	1023	906	939	28
KS04-01	881	756	794	10
KS04-03	1030	785	847	6
LR04-04	944	688	800	19
LO06-01	1020	713	824	43

6.1.1. Mafic garnet-orthopyroxene granulite from Labait (LB04-91)

Temperatures recorded by the zircons are significantly higher than the temperatures recorded by the rutile crystals (Fig. 14). Zircons returned temperatures between 906- 1023 °C, with a mean recorded temperature of 939 ± 44 °C, 1σ. Temperatures recorded by the rutile grains range from 622 to 785 °C. The mean rutile temperature is 637 ± 45 °C. This large difference in temperature recorded by the zircon and rutile implies slow cooling, which suggests that this xenolith is a sample of the present-day lower crust that experienced very high temperatures (based on the zircon results) and cooled slowly. The rutile crystals were frequently associated with ilmenite rims and lamellae (Fig. 15). Rutile grain 2 was almost entirely ilmenite with a small rutile zone located near the edge of the crystal (Fig. 16). The Zr concentration measured within the rutile zone returned a temperature of 819 °C (the highest temperature recorded by a rutile crystal in this sample). This temperature was not considered when analyzing the data because it was not acquired from a rutile grain, but from a rutile zone within an

ilmenite grain. The inclusion of this temperature in my data set would not affect my interpretation, because 819 °C is still significantly lower than the temperatures returned by the zircons.

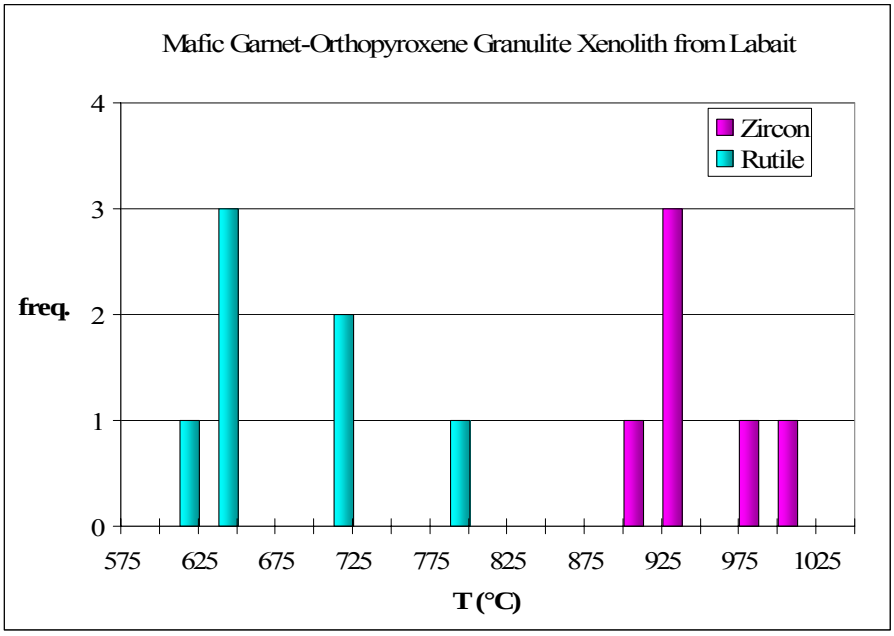

Fig. 14. Histogram showing the distribution of temperatures recorded by zircon and rutile in the mafic garnet-orthopyroxene granulite xenolith from Labait (sample LB04-91).

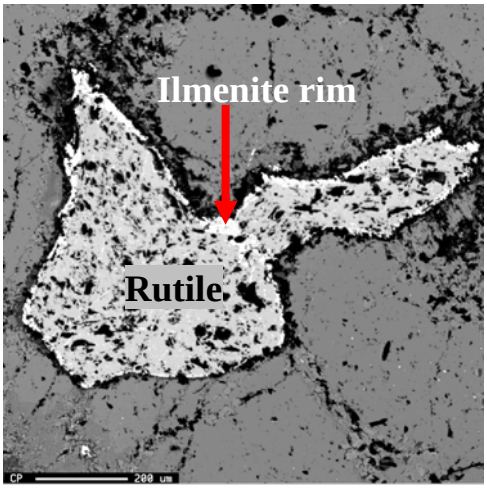

Fig. 15. BSE image of a rutile grain with ilmenite rims (lighter area along the edge of the grain) from the mafic garnet-orthopyroxene

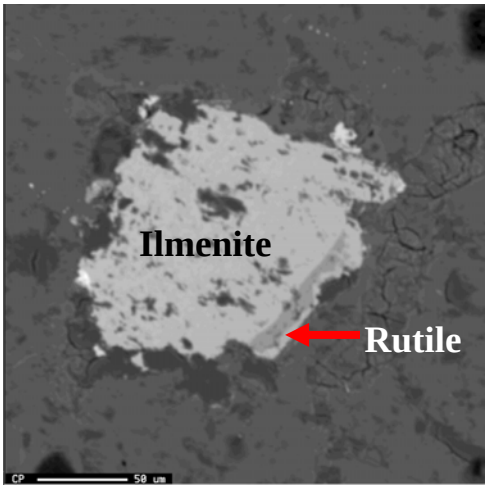

Fig. 16. BSE image of an ilmenite grain with a rutile zone (dark area along the right edge of the grain) from the mafic garnet-orthopyroxene

6.1.2. Garnet-biotite orthogneiss from Kisite (KS04-03)

The zircons in this sample displayed some of the hottest temperatures of any of the samples. The zircon temperatures that were recorded are variable, ranging from 785 to 1030 °C, with an average temperature of 852 ± 84 °C. The two highest temperatures, 1012 and 1026 °C, were calculated from peaks in Ti concentrations from zircons that displayed variable spatial distributions of Ti (Fig. 17). These peaks occur closer to the outside of the crystal, which is inconsistent with their origin as high-temperature igneous cores. CL images of the zircons confirmed the presence of igneous cores and zoning (Fig. 18). Other temperatures recorded by the zircons are between 785-912 °C, but like the mafic garnet-orthopyroxene granulite from Labait, the zircon temperatures are consistently greater than the temperatures calculated from the rutile crystals (Fig. 19). The range in rutile temperatures is 590 to 749 °C, with an average of 676 ± 42 °C. Again, this difference in rutile and zircon temperature suggests slow cooling and could be interpreted as isobaric cooling of the granulite in the present-day lower crust.

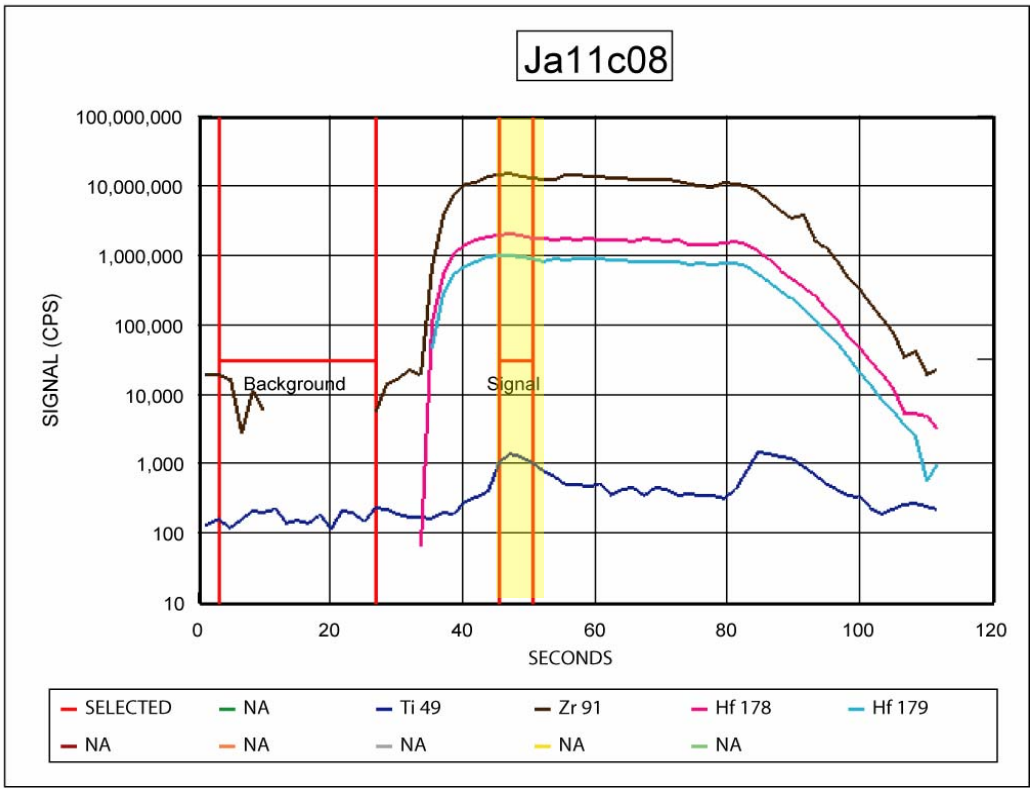

Fig. 17. Time-resolved spectrum of a zircon analysis from the garnet-biotite orthogneiss xenolith from Kisite (KS04-03) Note the ^{49}Ti peak within the highlighted area. The peak that occurs at approximately 50 seconds corresponded to a concentration of 114 ppm. The peak that occurs ~90 seconds begins to rise as Hf and Zr begin to fall, which suggests that we have ablated through the zircon and are ablating into an adjacent Ti-rich phase.

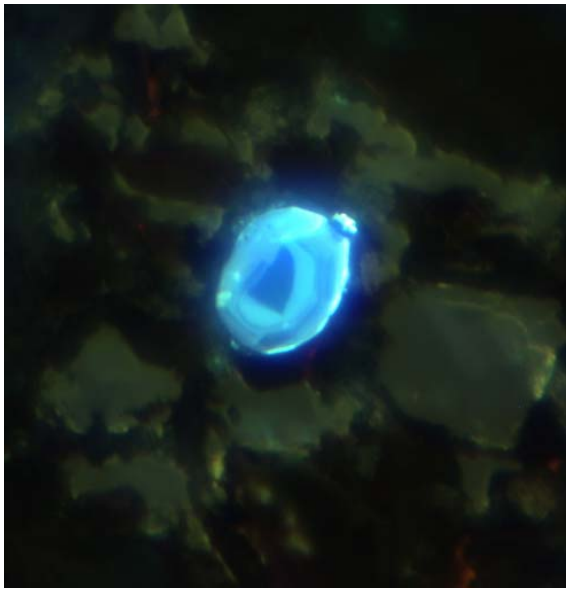

Fig. 18. CL image of a zircon displaying concentric zoning from the garnet-biotite orthogneiss xenolith from Kisite (KS04-03).

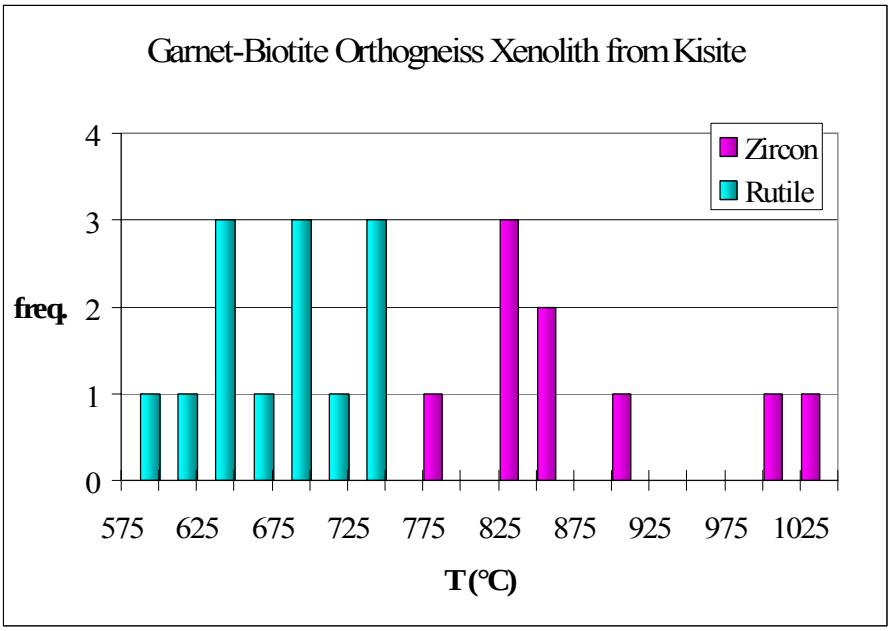

Fig. 19. Histogram showing the distribution of temperatures recorded by zircon and rutile in the garnet-biotite orthogneiss xenolith from Kisite (KS04-03).

6.1.3. Mafic garnet-orthopyroxene granulite from Kisite (KS04-01)

Sample KS04-01 yields zircon temperatures that range from 756 to 881 °C with a mean temperature of 794 ± 43 °C. Concentrations of Ti in the different zircons were fairly homogenous, resulting in a small range of recorded temperatures. Rutile temperatures range from 751 to 794 °C with an average temperature of 760 ± 14 °C. The ranges in temperature recorded by the zircon and rutile crystals overlap, as depicted in Fig. 20, and the average temperatures are the same, within uncertainty. The fact that the rutile yields roughly the same temperatures recorded by the zircon crystals implies cooling rates in excess of 10 °C/m.y. or even 100 °C/m.y. This suggests that the xenolith may have derived from a near-surface granulite terrane that experienced relatively quick cooling due to rapid uplift.

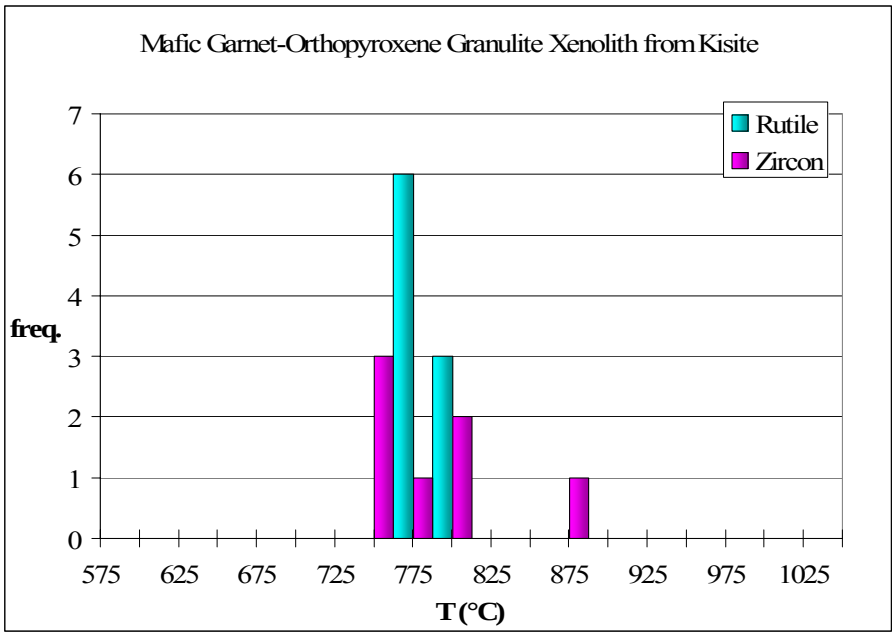

Fig. 20. Histogram showing the distribution of temperatures recorded by zircon and rutile in the mafic garnet-orthopyroxene granulite xenolith from Kisite (KS04-01).

6.2. Surface Sample Zircon and Rutile Temperatures and Interpretations

6.2.1. Graphite schist from Loibor Serrit (LR04-04)

Zircon temperatures range from 688 to 944 °C with a mean temperature of 800 ± 76 °C. The large variability in temperatures recorded by the zircons may be attributed to the presence of multiple populations of zircons, such as detrital zircons and metamorphic zircons. The temperatures recorded by the rutile crystals are relatively homogenous and range from 754 to 810 °C (mean = 791 ± 11 °C). Temperatures are plotted in Fig. 21. These temperatures, recorded by both the zircon and rutile, seem anomalously high for a mica-graphite schist, which again may be a consequence of multiple populations of zircons and/or retrograde metamorphism. The rutile crystals presumably formed during the metamorphic event, yet they recorded temperatures that are uncharacteristically high for a graphite schist. Conclusions about the cooling history of this sample cannot be made

until further analyses of the zircons are conducted. It would be useful to try to distinguish zircons from multiple populations (i.e. detrital versus metamorphic), which could be accomplished via zircon dating techniques, i.e. Pb-Pb evaporation and U-Pb SHRIMP, or other chemical analyses, assuming zircons with similar chemical signatures formed during the same event(s). For example, Ti-in-zircon thermometry could be applied to zircons that return dates of approximately 640 Ma (the time of peak metamorphism), and a conclusion can be made regarding the cooling history of this sample.

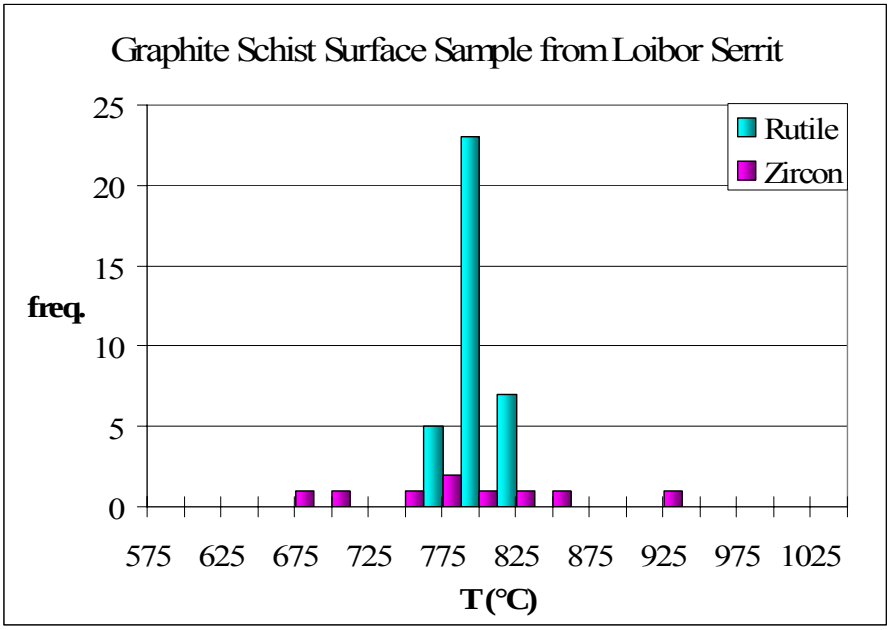

Fig. 21. Histogram showing the distribution of temperatures recorded by zircon and rutile in the graphite schist surface sample from Loibor Serrit (LR04-04).

6.2.2. Garnet amphibolite from Lolikisale (LO06-01)

This surface sample yields zircon temperatures that range from 713 to 1020 °C with an average temperature of 824 ± 121 °C. In two zircon analyses, as the laser ablated through the crystals, Ti concentration jumped dramatically and fell more gradually (Fig. 13). These peaks yielded the highest zircon temperatures for this sample (921 and 1020

°C). Other calculated temperatures range from 713 to 868 °C. Their highly variable temperatures result from zoning within the zircons. The EPMA was used to take BSE and CL images of several zircons to identify zoning, but no distinct zoning was evident (a few zircons looked somewhat heterogeneous in composition). Additional CL imaging of the zircons was conducted at the Smithsonian Institute. The zircons displayed "blocky" zoning, with several of the zircons displaying non-luminescent cores surrounded by brighter rims (Fig. 22). If the darker interiors are igneous cores, the high temperatures returned by the zircons may reflect the temperature conditions during which the igneous cores formed, in which case they may be ignored for purposes of this study. Rutile temperatures range from 651 to 765 °C with a mean temperature of 714 ± 23 °C. If we omit the two highest temperatures returned by the zircons, the recorded rutile and zircon temperatures overlap (Fig. 23), suggesting that the sample experienced relatively fast cooling and may have derived from the present day upper-crust.

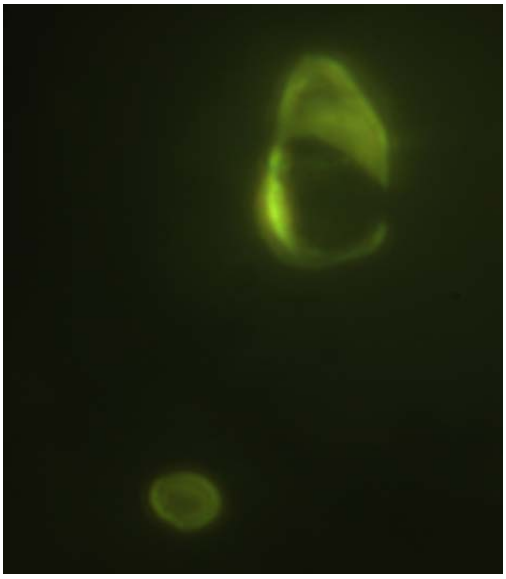

Fig. 22. CL image of zircons from the garnet amphibolite surface sample from Lolikisale displaying zoning. Note the non-luminescent cores and brighter rims.

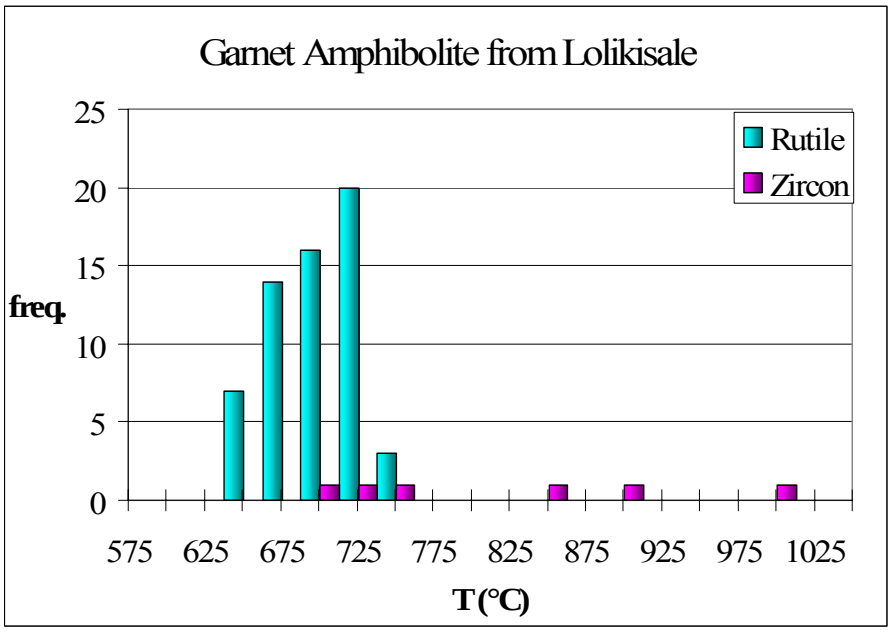

Fig. 23. Histogram showing the distribution of temperatures recorded by zircon and rutile in the garnet amphibolite surface sample from Lolikisale (LO06-01).

7. Conclusions

The mafic garnet orthopyroxene granulite xenolith from Labait and the garnet biotite orthogneiss xenolith from Kisite yield zircon temperatures that are significantly higher than those returned by the coexisting rutile. This suggests they experienced high T, cooled slowly and thus derived from the present-day lower crust. On the other hand, the mafic garnet-orthopyroxene granulite xenolith from Kisite yields zircon and rutile temperatures that are indistinguishable from each other, within error, and the zircons returned cooler temperatures than those of the garnet biotite orthogneiss from Kisite. This suggests that the xenolith formed at cooler metamorphic temperatures than the other Kisite xenolith, experienced more rapid cooling and therefore is a sample of the present-day upper crust.

The graphite schist from Loibor Serrit yields zircon temperatures that are both higher and lower than the temperatures returned by rutile. The large variability in the temperatures recorded by the zircons may be the consequence of analyzing multiple populations of detrital zircons, which could potentially return different temperatures. Rutile temperatures were relatively homogenous. The garnet rutile amphibolite from Lolikisale returned highly variable zircon temperatures as well, with the highest temperatures reflecting Ti-rich zones within the crystals. CL imaging on the EPMA displayed what appeared to be minor zoning in several zircons that was not visible in backscattered electron images. The different zones could potentially return different temperatures. The temperatures recorded by the rutile in this sample were fairly homogeneous. Further investigation of the two surface samples is necessary to draw any conclusions about the cooling histories of these two samples.

Acknowledgments

I would like to thank the many people who made this project possible. I could not have done it without the guidance and support of my advisors, Dr. Roberta Rudnick, Dr. Phil Piccoli, and Dr. William McDonough. I would also like to thank Dr. Sorena Sorensen for her generous assistance at the Smithsonian Institute. I would especially like to thank Dr. Roberta Rudnick for her endless patience and constant support and for giving me a once in a lifetime opportunity to join her on a trip to Tanzania. This project was a wonderful and memorable experience. Thank you all.

References

Appel P, Möller A, Schenk V (1998) High-pressure granulite facies metamorphism in the Pan-African belt of eastern Tanzania: P-T-t evidence against granulite formation by continent collision. *Journal of Metamorphic Geology* 16: 491-509.

Chesley JT, Rudnick RL, Lee C-T (1999) Re-Os systematics of mantle xenoliths from the East African Rift: Age, structure, and history of the Tanzanian craton. *Geochimica et Cosmochimica Acta* 63: 1203-1217.

Dodson MH (1973) Closure temperature in cooling geochronological and petrological systems. *Contr Mineral and Petrol* 40: 259-247.

Hausenberger CA, Bauernhofer AH, Hoinkes G, Wallbrecher E, and Mathu EM (2004) Pan-African high pressure granulites from SE-Kenya: Petrological and geothermobarometric evidence for a polycyclic evolution in the Mozambique belt. *Journal of African Earth Sciences* 40: 245-268.

Johnson SP, Cutten HNC, Muhongo S, De Waele B (2003) Neoarchaean magmatism and metamorphism of the western granulites in the central domain of the Mozambique belt, Tanzania: U-Pb shrimp geochronology and PT estimates. *Tectonophysics* 375: 125-145.

Jones A, Smith J, Dawson B, Hansen E (1983) Metamorphism, partial melting, and K-metasomatism of garnet-scapolite-kyanite granulite xenoliths from Lashaine, Tanzania. *Journal of Geology* 91: 143-165.

Kröner A, Muhongo S, Hegner E, Wingate MTD (2003) Single-zircon geochronology and Nd isotopic systematics of Proterozoic high-grade rocks from the Mozambique belt of southern Tanzania (Masasi area): implications for Gondwana assembly. *Journal of the Geological Society* 106: 745-757.

Lee C-T, Rudnick RL (1999) Compositionally stratified cratonic lithosphere: petrology and geochemistry of peridotite xenoliths from the Labait Volcano, Tanzania. *Proceedings of the VIIth International Kimberlite Conference*, pp. 503-521, Cape Town, South Africa, J.J. Gurney and S.R. Richardson, Eds. (Red Barn, Cape Town, South Africa, 1999).

Möller A, Mezger K, Schenk V (1998) Crustal age domains and the evolution of the continental crust in the Mozambique Belt of Tanzania: combined Sm-Nd, Rb-Sr, and Pb-Pb isotopic evidence. *Journal of Petrology* 39: 749-783.

Möller A, Mezger K, Schenk V (2000) U-Pb dating of metamorphic minerals: Pan-African metamorphism and prolonged slow cooling of high pressure granulites in Tanzania, East Africa. *Precambrian Research* 104: 123-146.

Muhongo S, Kröner A, Nemchin AA (2001) Single zircon evaporation and SHRIMP ages for granulite-facies rocks in the Mozambique Belt of Tanzania. *The Journal of Geology* 109: 171-189.

Prochaska W, Pohl W (1983) Petrochemistry of some mafic and ultramafic rocks from the Mozambique Belt, northern Tanzania. *Journal of African Earth Sciences* 1: 183-191.

Schenk V et al. (2005) Gondwana formation: A metamorphic view from the margins of the Congo Craton. *Geological Society of Australia Abstracts* 81.

Schmitz MD, Bowring SA (2002) Constraints on the thermal evolution of continental lithosphere from U-Pb accessory mineral thermochronometry of lower crustal xenoliths, southern Africa. *Contrib. Mineral. Petrol.* 144: 592-618.

Snoeyenbos DR, Williams ML, Hanmer S (1995) Archean high-pressure metamorphism in the western Canadian Shield. *Eur. J. Mineral.* 7: 1251-1272.

Sommer H, Kröner A, Hauzenberger C, Muhongo S, Wingate MTD (2003) Metamorphic petrology and zircon geochronology of high-grade rocks from the central Mozambique Belt of Tanzania: crustal recycling of Archean and Palaeoproterozoic material during the Pan-African orogeny. *Journal of Metamorphic Geology* 21: 915-934.

Stanley, Steven M. Earth System History. W.H. Freeman and Company, New York 1999.

Watson EB, Wark DA, Thomas JB (2005) Crystallization thermometers for zircon and rutile (preprint; will soon be submitted for publication).

Weeraratne D, Forsyth D, Fischer K, Nyblade A (2003) Evidence for an upper mantle plumes beneath the Tanzanian craton from Rayleigh wave tomography. *Journal of Geophysical Research* 108:10-1 - 10-14.

Winter, John D. An Introduction to Metamorphic Petrology. Prentice-Hall Inc., New Jersey 2001.

Appendix I

Rutile Analyses Data

Sample: Mafic garnet-orthopyroxene granulite xenolith from Labait (LB04-91)

Grain No.	ZrO_2 (wt%)	Zr (ppm)	Error (ppm)	TiO2 (wt%)	Ti (ppm)	FeO (wt%)	Fe (ppm)	Total (wt%)	Comment	Temp (ºC)	Error (ºC)
1	0.085	630	19	99.32	595279	0.01	87	99.62	Core	707	25
	0.093	691	20	100.46	602127	0.02	184	100.75	Core	716	25
	0.184	1365	29	99.63	597154	0.01	73	99.99	Core	785	28
	0.012	89	7	100.24	600820	0.02	135	100.56	Core	553	18
	0.100	740	21	68.11	408196	20.85	162060	92.41	Intermediate Gray Rim		
	0.048	356	15	54.57	327094	37.42	290896	92.57	Light Gray Rim		
	0.117	866	23	54.92	329172	37.53	291756	94.21	Intermediate Gray Rim		
2	0.250	1854	33	99.97	599169	0.56	4315	100.95	Intermediate Gray Rim	819	30
	0.022	166	10	52.88	316930	42.39	329498	95.82	Core		
	0.014	102	8	51.09	306203	44.32	344472	95.87	Core		
	0.031	229	12	52.97	317470	43.20	335816	96.66	Core		
3	0.038	279	13	101.12	606050	0.10	812	101.43	Core	637	22
	0.038	279	13	100.31	601245	0.04	280	100.60	Core	637	22
	0.017	123	9	58.93	353185	33.75	262318	93.22	Intermediate Gray Rim		
	0.012	91	8	58.68	351686	33.13	257554	92.32	Intermediate Gray Rim		
4	0.038	279	13	100.80	604130	0.10	746	101.01	Core	637	22
	0.032	233	12	100.03	599541	0.09	678	100.33	Core	622	21
	0.006	bd		32.23	193196	46.93	364830	95.50	Rim		
	0.000	bd		53.17	318661	38.96	302809	93.15	Light Gray Rim		
									ave.	677	
Key:	omitted	T_{max}/T_{min}	Ilmenite	Other phase					**med.**	**637**	
									std. dev.	60.5	

Rutile Analyses Data

Sample: Mafic garnet-orthopyroxene granulite xenolith from Kisite (KS04-01)

Grain No.	ZrO_2 (wt%)	Zr (ppm)	Error (ppm)	TiO_2 (wt%)	Ti (ppm)	FeO (wt%)	Fe (ppm)	Total (wt%)	Comment	Temp (ºC)	Error (ºC)
1	0.134	993	24	99.00	593357	0.34	2614	99.76	Core	751	27
	0.138	1024	25	100.49	602290	0.04	278	100.95	Core	755	27
	0.059	437	17	53.83	322611	35.98	279651	90.90	Rim		
	0.051	381	15	55.43	332200	37.00	287598	93.36	Rim		
2	0.188	1395	29	99.31	595250	0.16	1205	99.84	Core	787	28
	0.196	1452	29	99.48	596271	0.11	886	99.99	Core	792	28
	0.200	1479	30	97.14	582192	0.18	1362	97.68	Dark Gray Core	794	29
	0.050	370	15	53.87	322902	38.71	300926	93.31	Rim		
3	0.146	1081	25	102.36	613498	0.05	423	102.71	Core	760	27
	0.135	1001	24	101.52	608465	0.09	672	101.94	Core	752	27
	0.082	605	20	55.28	331308	36.05	280219	92.52	Core		
4	0.163	1206	27	99.54	596612	0.15	1150	100.30	Core	772	28
	0.143	1059	25	100.13	600109	0.20	1576	100.77	Core	758	27
	bd	bd	bd	50.50	302654	44.82	348362	96.11	Light Gray Rim		
									average	769	
Key:	omitted	T_{max}/T_{min}	Ilmenite	Other phase					**median**	**760**	
									stand dev	17.6	

Rutile Analyses Data

Sample: Garnet-biotite orthogneiss xenolith from Kisite (KS04-03)

Grain No.	ZrO_2 (wt%)	Zr (ppm)	Error (ppm)	TiO_2 (wt%)	Ti (ppm)	FeO (wt%)	Fe (ppm)	Total (wt%)	Comment	Temp (ºC)	Error (ºC)
1	0.060	444	16	99.99	599297	0.27	2068	100.45	Core	676	23
	0.068	504	17	99.97	599161	0.25	1962	100.43	Core	687	24
	0.052	386	15	100.15	600264	0.26	1991	100.60	Core	663	23
2	0.039	288	13	100.12	600053	0.29	2229	100.60	Core	639	22
	0.020	151	10	99.25	594844	0.28	2187	99.72	Core	590	20
	0.035	257	12	100.10	599980	0.28	2183	100.57	Core	630	21
3	0.119	877	23	99.87	598550	0.40	3097	100.53	Core	739	26
	0.103	761	22	100.09	599870	0.53	4135	100.85	Core	725	25
	0.038	281	13	98.64	591234	0.67	5204	99.49	Core	637	22
	0.108	799	21	67.60	405155	28.64	222608	96.95	Core Lamallae		
4	0.032	238	12	100.40	601776	0.54	4234	101.12	Core	624	21
	0.064	473	17	101.13	606118	0.61	4753	101.92	Core	681	23
	0.081	596	19	82.91	496926	14.69	114169	98.32	Core Lamallae		
5	0.128	948	24	99.75	597873	0.36	2835	100.38	Core	747	26
	0.131	970	24	99.31	595208	0.46	3594	100.12	Core	749	26
									ave.	676	
Key:	omitted	T_{max}/T_{min}	Ilmenite	Other phase					**med.**	**676**	
									std. dev.	51.8	

Rutile Analyses Data

Sample: Graphite schist surface sample from Loibor Serrit (LR04-04)

Grain No.	ZrO_2 (wt%)	Zr (ppm)	Error (ppm)	TiO_2 (wt%)	Ti (ppm)	FeO (wt%)	Fe (ppm)	Total (wt%)	Temp (ºC)	Error (ºC)
1	0.173	1281	5	97.16	582312	0.0185	144	97.35	778	28
	0.177	1308	5	98.42	589889	0.0259	201	98.62	780	28
	0.172	1275	5	98.18	588420	0.0235	183	98.37	778	28
2	0.149	1104	4	98.90	592767	0.0685	532	99.12	762	27
	0.138	1018	4	100.28	601044	0.0320	249	100.45	754	27
	0.148	1096	4	99.99	599287	0.0094	73	100.15	762	27
3	0.220	1625	6	98.16	588302	0.0102	79	98.39	804	29
	0.225	1663	6	97.93	586929	0.0094	73	98.16	807	29
	0.230	1701	6	98.73	591773	0.0188	146	98.98	810	29
4	0.174	1290	5	91.17	546412	0.0286	222	91.37	779	28
	0.165	1219	4	90.11	540056	0.0289	225	90.30	773	28
	0.159	1176	4	91.90	550784	0.0299	232	92.08	769	27
	0.181	1336	5	93.30	559209	0.0298	232	93.51	783	28
	0.176	1305	5	93.47	560240	0.0116	90	93.66	780	28
5	0.178	1315	5	98.72	591678	0.0767	596	98.97	781	28
6	0.185	1370	5	98.76	591896	0.0000	0	98.94	785	28
	0.181	1338	5	99.20	594570	**0.1119**	870	99.49	783	28
	0.177	1307	5	98.77	591989	0.0193	150	98.97	780	28
	0.189	1398	5	99.34	595406	0.0000	0	99.53	788	28
	0.196	1450	5	99.42	595855	0.0122	95	99.62	792	28
	0.194	1435	5	99.90	598751	0.0193	150	100.11	791	28
7	0.216	1602	6	98.26	588943	0.0358	278	98.51	803	29
	0.209	1547	6	98.14	588185	0.0152	118	98.36	799	29
	0.231	1713	6	97.77	586017	0.0201	156	98.03	810	29
8	0.176	1303	5	97.07	581814	0.0268	208	97.28	780	28
	0.186	1374	5	97.98	587228	0.0337	262	98.20	786	28
	0.199	1472	5	99.15	594250	0.0326	253	99.38	793	28
9	0.197	1455	5	99.74	597810	0.0029	23	99.94	792	28
	0.208	1536	6	98.84	592419	0.0000	0	99.05	798	29
	0.228	1689	6	99.46	596122	0.0219	170	99.71	809	29
10	0.210	1557	6	99.43	595942	0.0095	74	99.65	800	29
	0.196	1450	5	99.00	593393	0.0000	0	99.20	792	28
	0.222	1646	6	99.02	593494	0.0124	96	99.26	806	29
	0.198	1466	5	99.19	594477	0.0130	101	99.40	793	28
	0.210	1553	6	98.81	592215	0.0048	37	99.02	799	29
	0.195	1440	5	99.55	596664	0.0000	0	99.75	791	28

					ave.	788
Key:	omitted	T_{max}/T_{min}	Ilmenite	Other phase	**med.**	**791**
					std. dev.	14.2

Rutile Analyses Data

Sample: Garnet amphibolite surface sample from Lolikisale (LO06-01)

Grain No.	ZrO_2 (wt%)	Zr (ppm)	Error (ppm)	TiO_2 (wt%)	Ti (ppm)	FeO (wt%)	Fe (ppm)	Total (wt%)	Temp (ºC)	Error (ºC)
1	0.087	643	2	100.10	599973	0.1207	938	100.31	709	25
	0.073	538	2	100.58	602826	0.2258	1755	100.88	693	24
	0.000	0	0	54.35	325752	46.4389	360979	100.79		
	0.094	698	3	100.25	600837	0.2179	1694	100.56	717	25
	0.104	770	3	100.87	604589	0.1577	1226	101.13	726	25
	0.101	745	3	100.33	601342	0.1319	1025	100.56	723	25
	0.101	745	3	100.13	600160	0.1368	1063	100.37	723	25
	0.103	765	3	100.29	601091	0.1486	1155	100.54	726	25
	0.107	794	3	100.52	602447	0.1596	1241	100.78	729	26
	0.107	794	3	100.64	603220	0.1424	1107	100.89	729	26
	0.107	789	3	100.03	599532	0.1531	1190	100.29	729	25
2	0.115	854	3	100.73	603761	0.1796	1396	101.03	736	26
	0.108	803	3	99.36	595537	0.1920	1492	99.66	730	26
	0.091	677	2	100.65	603236	0.1437	1117	100.88	714	25
	0.099	735	3	100.52	602475	0.1123	873	100.73	722	25
	0.107	789	3	100.29	601106	0.1149	893	100.51	729	25
	0.102	752	3	100.60	602962	0.1571	1221	100.86	724	25
	0	0	0	53.84	322676	45.4542	353325	99.29		
	0.106	783	3	99.59	596884	0.1117	868	99.80	728	25
	57.640	426721	1536	1.85	11075	0.0034	26	59.49		
	0.123	912	3	100.10	599946	0.1010	785	100.32	743	26
	0.110	815	3	100.22	600658	0.1189	924	100.45	732	26
	0.101	749	3	99.58	596829	0.1288	1001	99.81	724	25
3	0.045	333	1	100.37	601551	0.1951	1517	100.61	651	22
	0.054	397	1	100.66	603285	0.1494	1161	100.86	666	23
	0.066	491	2	101.01	605405	0.1702	1323	101.25	684	24
	0.024	176	1	76.43	458102	23.5735	183242	100.03		
	0.467	3460	12	0.41	2462	0.0686	533	0.95		
	0.082	608	2	100.47	602161	0.1456	1132	100.70	704	24
	0.092	682	2	100.07	599756	0.1485	1154	100.31	715	25
	0.104	768	3	100.28	601010	0.1268	986	100.51	726	25
	0.110	814	3	100.44	602018	0.1567	1218	100.71	732	26
	0.113	834	3	100.40	601764	0.1509	1173	100.66	734	26
	0.113	835	3	100.09	599881	0.1641	1276	100.36	734	26
4	0.070	516	2	100.55	602629	0.2344	1822	100.85	689	24
	0.069	509	2	100.95	605081	0.1476	1147	101.17	688	24

	0.062	456	2	101.08	605834	0.1695	1318	101.31	678	23
	0.069	512	2	100.38	601663	0.1882	1463	100.64	688	24
	0.092	679	2	101.12	606056	0.1043	811	101.31	714	25
	0.106	783	3	100.68	603453	0.1173	912	100.91	728	25
	0.091	675	2	100.93	604922	0.1107	860	101.13	714	25
	0.025	185	1	25.66	153781	0.0721	560	25.75		
	0.009	68	0	53.03	317831	45.0793	350411	98.12		
	0.071	523	2	101.74	609816	0.1178	916	101.93	690	24
	0.081	602	2	100.22	600674	0.1456	1132	100.45	703	24
	0.048	356	1	100.75	603847	0.2821	2193	101.08	657	22
	0.081	601	2	100.82	604281	0.1034	804	101.01	703	24
5	0.067	496	2	100.32	601294	0.1960	1524	100.59	685	24
	0.123	908	3	100.35	601484	0.1260	979	100.60	742	26
	0.091	671	2	100.21	600617	0.1112	864	100.41	713	25
	0.059	436	2	100.43	601935	0.1095	851	100.60	674	23
	26.474	195991	706	58.00	347646	0.1207	938	84.60		
	31.367	232218	836	48.00	287670	0.3634	2825	79.73		
	0.066	486	2	100.12	600065	0.1973	1534	100.38	684	23
	0.088	649	2	100.30	601172	0.1464	1138	100.54	710	25
	0.066	489	2	99.72	597689	0.1203	935	99.91	684	23
	0.052	383	1	100.16	600322	0.3003	2334	100.51	663	23
	0.001	10	0	53.78	322336	44.6919	347399	98.47		
	0.06	444	2	99.97	599151	0.2572	1999	100.28	676	23
6	0.052	383	1	100.87	604578	0.2381	1851	101.16	663	23
	0.064	477	2	100.88	604647	0.2122	1649	101.16	682	23
	0.067	492	2	100.71	603610	0.1900	1477	100.97	685	24
	0.053	389	1	100.51	602429	0.2333	1813	100.80	664	23
	0.064	472	2	100.73	603753	0.2124	1651	101.01	681	23
7	0.123	907	3	100.10	599942	0.2923	2272	100.51	742	26
	0.133	986	4	100.33	601361	0.3080	2394	100.78	751	26
	0.111	820	3	100.04	599576	0.2601	2022	100.41	732	26
	0	0	0	53.09	318221	45.8202	356170	98.91		
	0.153	1133	4	100.61	602989	0.2647	2058	101.02	765	27
	0.143	1055	4	99.57	596783	0.2183	1697	99.93	758	27
	0.126	932	3	100.36	601543	0.2134	1659	100.70	745	26
								ave.	710	
Key:	omitted	T_{max}/T_{min}	Ilmenite	Other phase				**med.**	**714**	
								std. dev.	27.4	

Appendix II

Zircon Analyses Data

Garnet-biotite orthogneiss xenolith from Kisite

Run	Ti (ppm)	Zr (ppm)	Hf (ppm)	T (°C)	Comments	t on peak (s)
Ja11c10	16	431756	14143	**785**	KS04-03 Z#5	57.8
Ja11c07	27	443197	9811	837	KS04-03 Z#7 spot 2	39.1
Ja11c09	28	435804	9099	841	KS04-03 Z#8 spot 1	37.4
Ja11c08	29	446343	11377	847	KS04-03 Z#4, zone 2	23.8
Ja11c06	31	426236	9539	853	KS04-03 Z#7 spot 1	34
Ja11c05	32	448348	13512	857	KS04-03 Z#2-1	39.1
Ja11c04	52	409852	11289	912	KS04-03 Z#2 spot 2	10.2
Ja11c08	114	445031	11377	1015	KS04-03 Z#4, zone 1	5.1
Ja11c04	126	432912	11289	**1030**	KS04-03 Z#2 spot 2	5.1
average	30	852				
median	**29**	**847**				
stdev	6	84				

Mafic garnet-orthopyroxene granulite from Kisite

Run	Ti (ppm)	Zr (ppm)	Hf (ppm)	T (°C)	Comments	t on peak (s)
Ja11d05	12	487559	12844	**756**	KS04-01 Z#14, spot 2	13.6
Ja11d04	13	487559	12912	768	KS04-01 Z#14, spot 1	15.3
Ja11d06	14	487559	10469	772	KS04-01 Z#15	18.7
Ja11d09	17	487559	12819	794	KS04-01 Z#21	13.6
Ja11d08	22	487559	12875	818	KS04-01 Z#20, zone 2	10.2
Ja11d10	24	487559	13094	825	KS04-01 Z#23	20.4
Ja11d08	39	487559	13217	**881**	KS04-01 Z#20, zone 1	3.4
average	20	809				
median	**17**	**794**				
stdev	10	43				

Mafic garnet-orthopyroxene granulite from Labait

Run	Ti (ppm)	Zr (ppm)	Hf (ppm)	T (°C)	Comments	t on peak (s)
Fe16a03	49	479111	12683	**906**	LB04-91, zirc. 1	40.8
Fe16a05	63	426835	10599	936	LB04-91, zirc. 2.2	51.0
Fe16a08	63	414232	12216	937	LB04-91, zirc. 4.2	35.7
Fe16a07	65	393065	11389	941	LB04-91, zirc. 4.1	28.9
Fe16a04	101	391760	10822	999	LB04-91, zirc. 2.1	45.9

Fe16a06	120	403081	11099	**1023**	LB04-91, zirc. 3	20.4
average	77	962				
median	**64**	**939**				
stdev	28	44				

Graphite schist from Loibor Serrit

Run	Ti (ppm)	Zr (ppm)	Hf (ppm)	T (°C)	Comments	t on peak (s)
Fe16b10	5	361763	8318	**688**	LR04-04 zirc 6	28.9
Fe16b16	7	492295	9422	714	LR04-04 zirc 10	15.3
Fe16b14	14	459418	10251	773	LR04-04 zirc 8.2	17.0
Fe16b09	17	410053	9451	794	LR04-04 zirc 5	8.5
Fe16b08	18	441091	10436	800	LR04-04 zirc 1.2	23.8
Fe16b12	19	465398	10974	801	LR04-04 zirc 7a.2	32.3
Fe16b07	26	439404	10436	836	LR04-04 zirc 1	25.5
Fe16b11	33	459956	10974	859	LR04-04 zirc 7a.1	20.4
Fe16b13	67	449040	10251	**944**	LR04-04 zirc 8.1	27.2
average	23	822				
median	**18**	**800**				
stdev	19	76				

Garnet amphibolite from Lolikisale

Run	Ti (ppm)	Zr (ppm)	Hf (ppm)	T (°C)	Comments	t on peak (s)
Ma31b08	7	488226	8811	**713**	LO06-1 zirc 4	10.4
Ma31b06	10	423704	7985	739	LO06-1 zirc 3.1	6.9
Ma31b11	11	487584	9236	754	LO06-1 zirc 8	1.7
Ma31b07	35	450987	9102	868	LO06-1 zirc 3.2	6.9
Ma31b09	56	491060	10230	921	LO06-1 zirc 5	12.2
Ma31b05	118	520318	10830	**1020**	LO06-1 zirc 1	8.7
average	39	881				
median	**23**	**824**				
stdev	21	121				

Key:	xxx	**xxx**	
	internal std	high/low	t < 10 s